PROGRESS IN PHOTOVOLTAICS: RESEARCH AND APPLICATIONS
Prog. Photovolt: Res. Appl. 2003; **11**:47–62 (DOI: 10.1002/pip.459)

Applications

Comparative Study of Maximum Power Point Tracking Algorithms

D. P. Hohm and M. E. Ropp*,†
Electrical Engineering Department, South Dakota State University, Brookings, SD 5700-2220, USA

Maximum power point trackers (MPPTs) play an important role in photovoltaic (PV) power systems because they maximize the power output from a PV system for a given set of conditions, and therefore maximize the array efficiency. Thus, an MPPT can minimize the overall system cost. MPPTs find and maintain operation at the maximum power point, using an MPPT algorithm. Many such algorithms have been proposed. However, one particular algorithm, the perturb-and-observe (P&O) method, claimed by many in the literature to be inferior to others, continues to be by far the most widely used method in commercial PV MPPTs. Part of the reason for this is that the published comparisons between methods do not include an experimental comparison between multiple algorithms with all algorithms optimized and a standardized MPPT hardware. This paper provides such a comparison. MPPT algorithm performance is quantified through the MPPT efficiency. In this work, results are obtained for three optimized algorithms, using a microprocessor-controlled MPPT operating from a PV array and also a PV array simulator. It is found that the P&O method, when properly optimized, can have MPPT efficiencies well in excess of 97%, and is highly competitive against other MPPT algorithms. Copyright © 2002 John Wiley & Sons, Ltd.

KEY WORDS: maximum power point tracking; power electronics; digital control; MPPT efficiency; experimental comparison; microcontroller

INTRODUCTION

A PV array under constant uniform irradiance has a current–voltage (*I–V*) characteristic like that shown in Figure 1. There is a unique point on the curve, called the maximum power point (MPP), at which the array operates with maximum efficiency and produces maximum output power. When a PV array is directly connected to a load (a so-called 'direct-coupled' system), the system's operating point will be at the intersection of the *I–V* curve of the PV array and load line shown in Figure 1.

In general, this operating point is not at the PV array's MPP, which can be clearly seen in Figure 1. Thus, in a direct-coupled system, the PV array must usually be oversized to ensure that the load's power requirements can be supplied. This leads to an overly expensive system.

To overcome this problem, a switch-mode power converter, called a maximum power point tracker (MPPT), can be used to maintain the PV array's operating point at the MPP. The MPPT does this by controlling the PV

*Correspondence to: Michael Ropp, Electrical Engineering Department HH205, South Dakota State University, Brookings, SD 57007-2220, USA.
†E-mail: michael_ropp@sdstate.edu

Published online 22 November 2002

Received 12 February 2002
Revised 2 June 2002

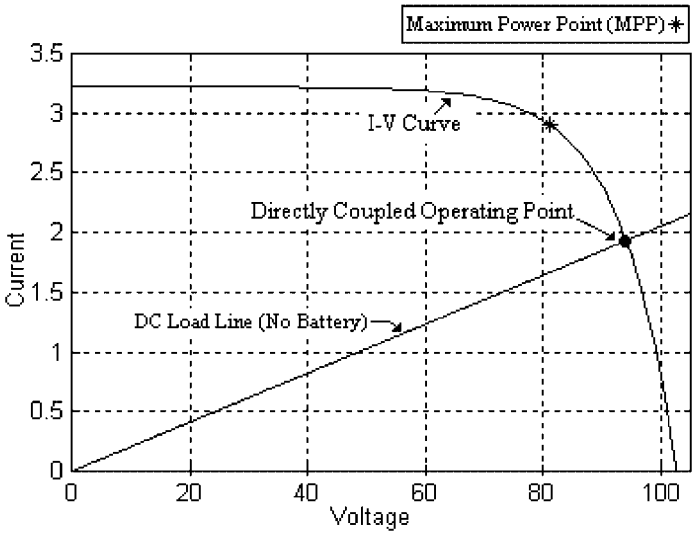

Figure 1. Typical current–voltage curve for a PV array

array's voltage or current independently of those of the load. If properly controlled by an MPPT algorithm, the MPPT can locate and track the MPP of the PV array. However, the location of the MPP in the *I–V* plane is not known *a priori*. It must be located, either through model calculations or by a search algorithm. The situation is further complicated by the fact that the MPP depends in a nonlinear way on irradiance and temperature, as illustrated in Figure 2. Figure 2(a) shows a family of PV *I–V* curves under increasing irradiance, but at constant temperature, and Figure 2(b) shows *I–V* curves at the same irradiance values, but a higher temperature. Note the change in the array voltage at which the MPP occurs.

A number of MPPT control algorithms have been proposed. One algorithm, the perturb-and-observe (P&O) algorithm, is by far the most commonly used in commercial MPPTs. However, there is as yet no consensus on which algorithm is 'best', and many authors have suggested that perhaps the P&O algorithm is inferior to others. This lack of consensus stems in part from the fact that the literature contains no comparisons of absolute efficiencies of MPPT algorithms, with all algorithms using optimized parameters and operating on a standardized MPPT hardware. Most of the reported comparisons are made between an MPPT algorithm and a direct-coupled system[1,2] or between an MPPT algorithm and a converter designed for a fixed operating point.[3] Others

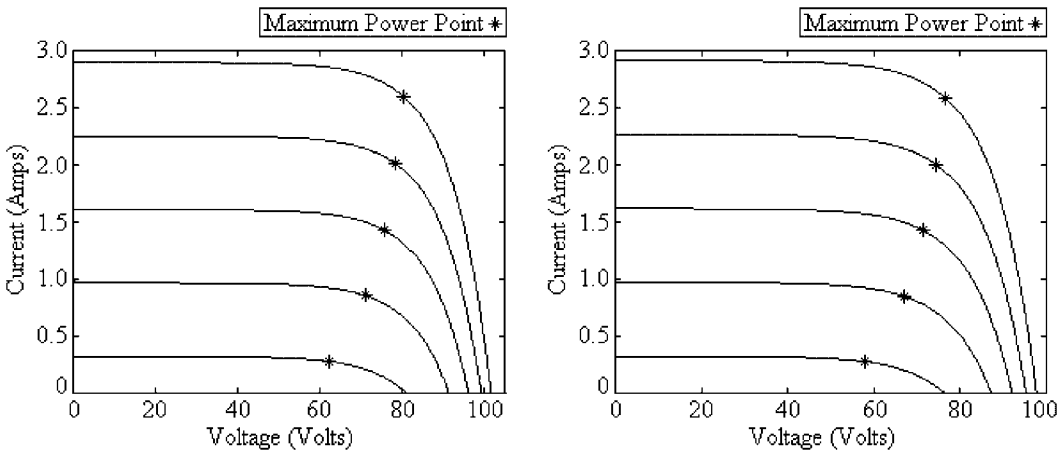

Figure 2. (a) PV array voltage–current at 40°C at different irradiance levels; (b) PV array voltage–current at 50°C at different irradiance levels

Table I. Summary of previously reported MPPT efficiencies for the four algorithms considered here

Reference	Reported MPPT efficiency (%)			
	Perturb-and-observe	Incremental conductance	Constant voltage	Parasitic capacitance
6	81·5	89·9		
5	85·0	88·0	73·0	
12			85·0	
14				99·8

report comparisons of one algorithm with another, but these generally compare an algorithm under test with fully optimized parameters against a baseline algorithm (usually P&O), the parameters of which are not described and appear not to be optimized.[4–6]

The purpose of this work is to obtain such an experimental comparison and to suggest which MPPT control algorithm is the most effective on the basis of MPPT efficiency, which is defined[6] as:

$$\eta_{\mathrm{MPPT}} = \frac{\int_0^t P_{\mathrm{actual}}(t)\mathrm{d}t}{\int_0^t P_{\max}(t)\mathrm{d}t} \tag{1}$$

where P_{actual} is the actual (measured) power produced by the PV array under the control of the MPPT, and $P_{\max}$ is the true maximum power the array could produce under a given temperature and irradiance. In this work, only MPPT algorithms that could presently be implemented in a low-cost MPPT were considered. Fuzzy logic and DSP-based systems were therefore excluded, and the following MPPT algorithms were chosen for further investigation:

- perturb and observe (P&O)
- incremental conductance (INC)
- parasitic capacitance (PC)
- constant voltage (CV)

For each of these algorithms, there is a previously reported MPPT efficiency in the literature. A summary of these results is given in Table I.

DESCRIPTION OF MPPT ALGORITHMS

Perturb-and-observe

The perturb and observe (P&O) algorithm is the most commonly used in practice because of its ease of implementation.[7] The most basic form of the P&O algorithm operates as follows. Consider Figure 3, which shows a family of PV array power curves as a function of voltage (*P–V* curves), at different irradiance (*G*) levels, for uniform irradiance and constant temperature. As previously described, these curves have global maxima at the MPP. Assume the PV array to be operating at point A in Figure 3, which is far from the MPP. In the P&O algorithm, the operating voltage of the PV array is perturbed by a small increment, and the resulting change in power, ΔP, is measured. If ΔP is positive, then the perturbation of the operating voltage moved the PV array's operating point closer to the MPP. Thus, further voltage perturbations in the same direction (that is, with the same algebraic sign) should move the operating point toward the MPP. If ΔP is negative, the system operating point has moved away from the MPP, and the algebraic sign of the perturbation should be reversed to move back toward the MPP.

The advantages of this algorithm, as stated before, are simplicity and ease of implementation. However, P&O has limitations that reduce its MPPT efficiency. One such limitation is that as the amount of sunlight decreases, the *P–V* curve flattens out, as seen in Figure 3. This makes it difficult for the MPPT to discern the location of the MPP, owing to the small change in power with respect to the perturbation of the voltage. Another fundamental

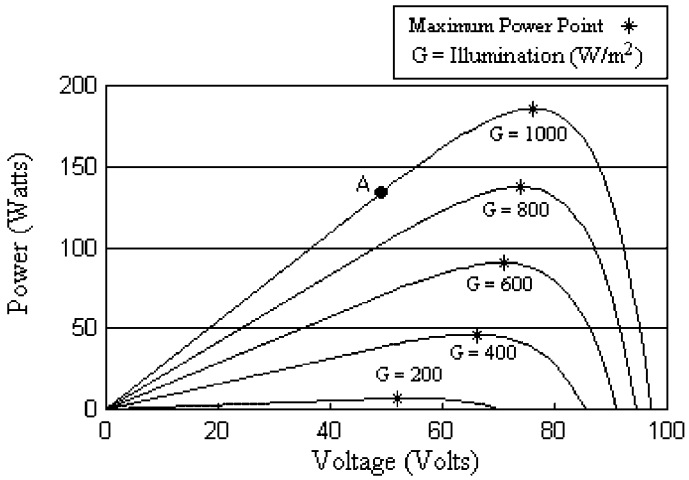

Figure 3. Photovoltaic array power–voltage relationship

drawback of P&O is that it cannot determine when it has actually reached the MPP. Instead, it oscillates around the MPP, changing the sign of the perturbation after each ΔP measurement. Also, it has been shown that P&O can exhibit erratic behavior under rapidly changing irradiance levels.[8] Figure 4 shows a close-up view of the solar array *P–V* characteristic near the MPP. Consider the case in which the irradiance is such that it generates *P–V* curve 1 in Figure 4. The MPPT is oscillating around the MPP from point B to A to C to A and so on. Then, assume the irradiance increases and the *P–V* curve of the array moves to curve 2. If, during the rapid increase in solar irradiance and output power, the MPPT was perturbing the operating point from point A to point B, the MPPT would actually move from A to D. As seen in Figure 4, this results in a positive ΔP, and the MPPT will continue perturbing in the same direction, toward point F. If the irradiance is still rapidly increasing, the PV power curve will move to G on curve 3 instead of to F on curve 2. Again the MPPT will see a positive ΔP and will assume it is moving towards the MPP, continuing to perturb to point I. From points A to D to G to I the MPPT is continually moving away from the MPP, decreasing the efficiency of the P&O algorithm. This situation can occur on partly cloudy days, when MPP tracking is most difficult, owing to the frequent movement of the MPP.

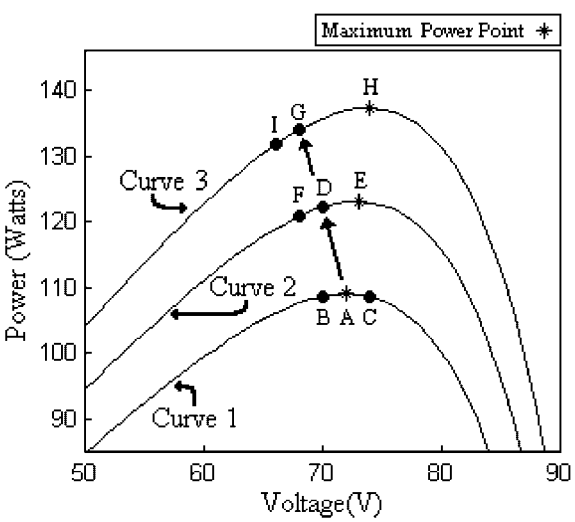

Figure 4. Illustration of erratic behavior of P&O under rapidly increasing irradiance

Several improvements of the P&O algorithm have been proposed.[9] One of the simplest entails the addition of a 'waiting' function that causes a momentary cessation of perturbations if the algebraic sign of the perturbation is reversed several times in a row, indicating that the MPP has been reached. This reduces the oscillation about the MPP in the steady state and improves the algorithm's efficiency under constant irradiance conditions. However, it also makes the MPPT slower to respond to changing atmospheric conditions, worsening the erratic behavior on partly cloudy days. Another modification involves measuring the array's power P_1 at array voltage V_1, perturbing the voltage and again measuring the array's power, P_2, at the new array voltage V_2, and then changing the voltage back to its previous value and remeasuring the array's power, P_1', at V_1. From the two measurements at V_1, the algorithm can determine whether the irradiance is changing. Again, as with the previous modifications, increasing the number of samples of the array's power slows the algorithm down. Also, it is possible to use the two measurements at V_1 to make an estimate of how much the irradiance has changed between sampling periods, and to use this estimate in deciding how to perturb the operating point. This, however increases the complexity of the algorithm, and also slows the operation of the MPPT.

Constant voltage and current

The basis for the constant voltage (CV) algorithm is the observation from *I–V* curves like those in Figure 1 that the ratio of the array's maximum power voltage, V_{MPP}, to its open-circuit voltage, V_{OC}, is approximately constant; in other words:

$$\frac{V_{MPP}}{V_{OC}} \cong K < 1 \tag{2}$$

The constant voltage algorithm can be implemented using the flowchart shown in Figure 5. The solar array is temporarily isolated from the MPPT, and a V_{OC} measurement is taken. Next, the MPPT calculates the correct operating point using Equation (2) and the preset value of K, and adjusts the array's voltage until the calculated V_{MPP} is reached. This operation is repeated periodically to track the position of the MPP.

Although this method is extremely simple, it is difficult to choose the optimal value of the constant K. The literature reports success with K values ranging from 73 to 80%.[10–12] Figure 6 shows the actual K values required for a given PV array over a temperature range of 0–60°C and irradiance levels from 200 to 1000 W/m^2. These curves were calculated using the *I–V* relationship for a PV cell given in Equations (3, 4 and 5).

$$I = I_L - I_{OS}\left[\exp\frac{q}{Ak_BT}\{V + IR\} - 1\right] \tag{3}$$

$$I_{OS} = I_{OR}\left(\frac{T}{T_R}\right)\exp\left[\frac{qE_G}{Ak_B}\left(\frac{1}{T_R} - \frac{1}{T}\right)\right] \tag{4}$$

$$I_L = \left(\frac{G}{1000}\right)\left[I_{SC} + K_{T,I}(T - T_R)\right] \tag{5}$$

Equation (3) is the Shockley equation for an illuminated pn junction. A is the diode ideality factor, q is the charge on an electron, and R is the PV array's series resistance. (The shunt resistance has been assumed large enough to be accurately approximated as infinite.) Equation (4) accounts for the temperature dependency of the reverse saturation current I_{OS}. I_{OS} is a function of the reference reverse saturation current I_{OR} at the standard

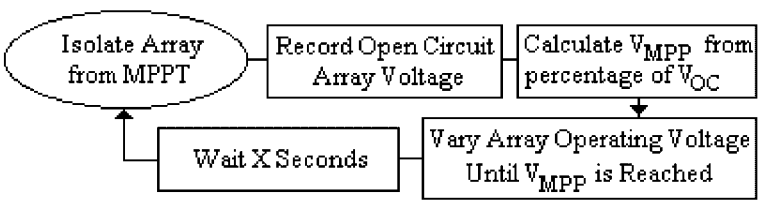

Figure 5. Constant voltage algorithm flowchart

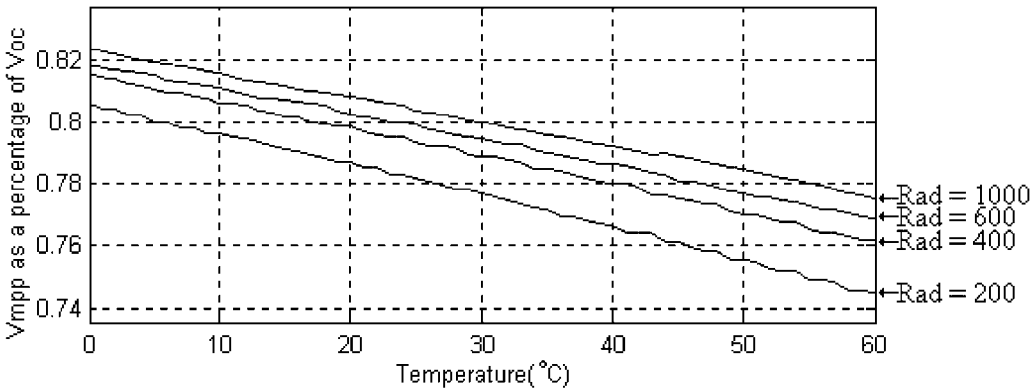

Figure 6. V_{MPP} as a percentage of V_{OC} as functions of temperature and irradiance

test condition reference temperature T_R (25°C), E_G, the bandgap of the semiconductor used, the measured cell temperature T(°C), Boltzmann's constant k_B, and the charge on an electron q. Equation (5) gives the light-generated current I_L as a function of irradiance G (W/m^2), the array's short-circuit current at standard test conditions I_{SC}, the temperature coefficient for current of the array $K_{T,I}$ (A/°C), (which is typically very small), and the array temperature T(°C). Figure 6 indicates that the ratio K is not constant, but in fact depends on temperature and irradiance and varies by as much as 8% (absolute) over the entire range of conditions.

Constant voltage control can be easily implemented with analog hardware. However, its MPPT tracking efficiency is low relative to those of other algorithms. Reasons for this include the aforementioned error in the value of K, and the fact that measuring the open-circuit voltage requires a momentary interruption of PV power. It is possible to dynamically adjust the value of K, but that requires a search algorithm and essentially ends up being the same as P&O.

It is also possible to use a constant current MPPT algorithm that approximates the MPP current as a constant percentage of the short-circuit current.[13] To implement this algorithm, a switch is placed across the input terminals of the converter and switched on momentarily. The short-circuit current is measured and the MPP current is calculated, and the PV array output current is then adjusted by the MPPT until the calculated MPP current is reached. This operation is repeated periodically. However, constant voltage control is normally favored because of the relative ease of measuring voltages, and because open-circuiting the array is simple to accomplish, but it is not practically possible to short-circuit the array (i.e., to establish zero resistance across the array terminals) and still make a current measurement.

Pilot cell

In the pilot cell MPPT algorithm, the constant voltage or current method is used, but the open-circuit voltage or short-circuit current measurements are made on a small solar cell, called a pilot cell, that has the same characteristics as the cells in the larger solar array.[13] The pilot cell measurements can be used by the MPPT to operate the main solar array at its MPP, eliminating the loss of PV power during the V_{OC} or I_{SC} measurement. However, the problem of a lack of a constant K value is still present. Also, this method has a logistical drawback in that the solar cell parameters of the pilot cell must be carefully matched to those of the PV array it represents. Thus, each pilot cell/solar array pair must be calibrated, increasing the energy cost of the system.

Incremental conductance

The incremental conductance algorithm is derived by differentiating the PV array power with respect to voltage and setting the result equal to zero.[6] This is shown in Equation (5).

$$\frac{dP}{dV} = \frac{d(VI)}{dV} = I + V\frac{dI}{dV} = 0 \text{ at the MPP} \tag{5}$$

Rearranging Equation (5) gives

$$-\frac{I}{V}=\frac{\mathrm{d}I}{\mathrm{d}V} \tag{6}$$

Note that the left-hand side of Equation (6) represents the opposite of the PV array's instantaneous conductance, while the right-hand side represents its incremental conductance. Thus, at the MPP, these two quantities must be equal in magnitude, but opposite in sign. If the operating point is off of the MPP, a set of inequalities can be derived from Equation (6) that indicates whether the operating voltage is above or below the MPP voltage. These relationships[6] are summarized in Equations (7a, b and c).

$$\frac{\mathrm{d}I}{\mathrm{d}V}=-\frac{I}{V};\quad\left(\frac{\mathrm{d}P}{\mathrm{d}V}=0\right) \tag{7a}$$

$$\frac{\mathrm{d}I}{\mathrm{d}V}>-\frac{I}{V};\quad\left(\frac{\mathrm{d}P}{\mathrm{d}V}>0\right) \tag{7b}$$

$$\frac{\mathrm{d}I}{\mathrm{d}V}<-\frac{I}{V};\quad\left(\frac{\mathrm{d}P}{\mathrm{d}V}<0\right) \tag{7c}$$

Equation 7(a) is a repeat of Equation (6) for convenience. Equations 7(b and c) are used to determine the direction in which a perturbation must occur to move the operating point toward the MPP, and the perturbation is repeated until Equation 7(a) is satisfied. Once the MPP is reached, the MPPT continues to operate at this point until a change in current is measured. This change in current will correlate to a change in irradiance on the array. As shown in Figure 3, as the irradiance on the array increases, the MPP moves to the right with respect to the array voltage. To compensate for this movement of the MPP, the MPPT must increase the array's operating voltage. The opposite is true when a decrease in irradiance is detected (via a decrease in the measured current).

Figure 7 shows a flowchart for the incremental conductance algorithm.[6] The present value and the previous value of the solar array voltage and current are used to calculate the values of dI and dV. If $\mathrm{d}V=0$ and $\mathrm{d}I=0$, then the atmospheric conditions have not changed and the MPPT is still operating at the MPP. If $\mathrm{d}V=0$ and $\mathrm{d}I>0$, then the amount of sunlight has increased, raising the MPP voltage. This requires the MPPT to increase

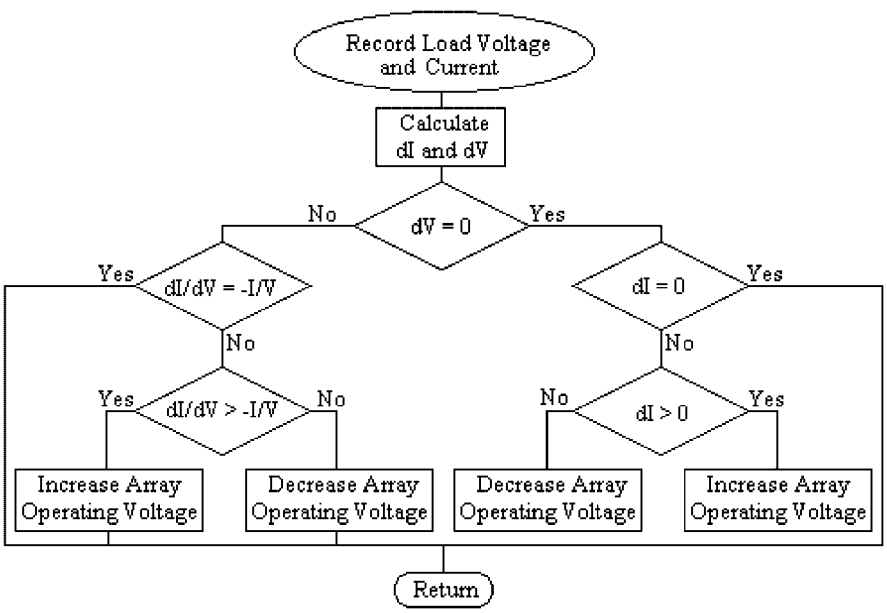

Figure 7. Incremental conductance algorithm flowchart

the PV array operating voltage to track the MPP. Conversely, if $dI < 0$, the amount of sunlight has decreased, lowering the MPP voltage and requiring the MPPT to decrease the PV array operating voltage. If the changes in voltage and current are not zero, the relationships in Equations 7(b,c) can be used to determine the direction in which the voltage must be changed in order to reach the MPP. If $dI/dV > -I/V$, then $dP/dV > 0$, and the PV array operating point is to the left of the MPP on the *P–V* curve. Thus, the PV array voltage must be increased to reach the MPP. Similarly, if $dI/dV < -I/V$, then $dP/dV < 0$ and the PV array operating point lies to the right of the MPP on the *P–V* curve, meaning that the voltage must be reduced to reach the MPP. Herein lies a primary advantage of incremental conductance over the perturb-and-observe algorithm: incremental conductance can actually calculate the direction in which to perturb the array's operating point to reach the MPP, and can determine when it has actually reached the MPP. Thus, under rapidly changing conditions, it should not track in the wrong direction, as P&O can, and it should not oscillate about the MPP once it reaches it.

Parasitic capacitance

The parasitic capacitance algorithm is similar to incremental conductance, except that the effect of the solar cells' parasitic junction capacitance C_P, which models charge storage in the *p–n* junctions of the solar cells, is included. By adding this capacitance to the lighted diode equation, Equation (3), and representing the capacitance using $i(t) = C dV/dt$, Equation (8) is obtained.[14]

$$I = I_L - I_O\left[\exp\left(\frac{V_P + R_S I}{a}\right) - 1\right] + C_P\frac{dv_P}{dt} = F(v_P) + C_P\frac{dv_P}{dt} \tag{8}$$

On the far right of Equation (8), the equation is rewritten to show the two components of I, a function of voltage $F(v_P)$ and the current in the parasitic capacitance. Using this notation, the incremental conductance of the array g_P can be defined as $dF(v_P)/dv_P$ and the instantaneous conductance of the array, g_L can be defined as $-F(v_P)/v_P$. The MPP is located at the point where $dP/dv_P = 0$. Multiplying Equation (8) by the array voltage v_P to obtain array power and differentiating the result, the equation for the array power at the MPP is obtained:[14]

$$\frac{dF(v_P)}{dv_P} + C_P\left(\frac{\dot{V}}{V} + \frac{\ddot{V}}{\dot{V}}\right) + \frac{F(v_P)}{v_P} = 0 \tag{9}$$

The three terms in Equation (9) represent the instantaneous conductance, the incremental conductance, and the induced ripple from the parasitic capacitance. The first and second derivatives of the array voltage take into account the AC ripple components generated by the converter. The reader will note that if C_P is equal to zero, this equation simplifies to that used for the incremental conductance algorithm. Since the parasitic capacitance is modeled as a capacitor connected in parallel with the individual solar cells, connecting the cells in parallel will increase the effective capacitance seen by the MPPT. From this, the difference in MPPT efficiency between the parasitic capacitance and incremental conductance algorithms should be at a maximum in a high-power solar array with many parallel modules.

The array conductance is easily calculated, since it is just the ratio of the instantaneous array current to the instantaneous array voltage. Obtaining the array differential conductance is more difficult, but it can be done[14] using Equation (10):

$$g_P = \frac{P_{GP}}{V_O^2} = \frac{\frac{1}{2}\sum_{n=1}^{\infty}\left[a_n^i \cdot a_n^v + b_n^i \cdot b_n^v\right]}{\frac{1}{2}\sum_{n=1}^{\infty}\left[\left(a_n^v\right)^2 + \left(b_n^v\right)^2\right]} \tag{10}$$

where P_{GP} is the average ripple power, V_O is the magnitude of the voltage ripple, and $a_n^i, a_n^v, b_n^i, b_n^v$ are the coefficients of the Fourier series of the PV array voltage and current ripples. The values of P_{GP} and V_O^2 may be obtained from a circuit configuration like that seen in Figure (8).[14] The inputs to the circuit are the measured array current and voltage. The high-pass filters remove the DC component of V_{PV}. The two multipliers generate

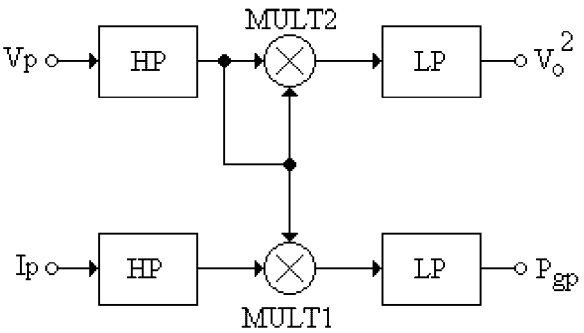

Figure 8. Circuitry used to implement the parasitic capacitance method[14]

the AC V_O^2 and AC P_{gP}, which are then filtered by the low-pass filters, leaving behind the DC components of V_O^2 and P_{gP}. From Equation (10), the ratio of these two values is equal to the array conductance, which can then be used in conjunction with Equations (7) until the array differential conductance and the array conductance are equal.

Model-based MPPT algorithms

If the values of the parameters in Equation (3) are known for a given solar cell, the solar cell current and voltage could be calculated from measurements of the light incident on and temperature of the solar cell. The maximum power voltage could then be calculated directly, and the PV array operating voltage could be simply set equal to V_{MPP}. Such an algorithm is commonly called a model-based MPPT algorithm. Although appealing, model-based MPPT is usually not practical because the values of the cell parameters are not known with certainty, and in fact can vary significantly between cells from the same production run. In addition, the cost of an accurate light sensor (pyranometer) can by itself make this MPPT scheme unfeasible.

EXPERIMENTAL PROCEDURE

Description of the MPPT testbed hardware

To facilitate the comparison of MPPT algorithms, a 250-W, microcontroller-based MPPT was designed and built. The use of a Motorola HC11 microcontroller allowed many MPPT algorithms to be compared using the same hardware, and also facilitated optimization of all algorithms. Figure 9 shows a schematic diagram of the MPPT. The measured load and array voltages and currents are fed into the voltage-conditioning block, which scales and offsets the voltages to the desired levels for the analog-to-digital converter. The MPPT algorithm under test is programmed into the microcontroller. Using the MPPT algorithm and the inputs just described, the microcontroller calculates the correct control signal for the main power circuit. This is output in digital form to the control circuitry block. The control circuitry block converts the digital number into an analog control signal, which in turn drives the main power circuit. This power circuit is a DC–DC buck (step-down) converter, selected because the PV array voltage being used is higher than the desired output voltage for the load and battery bank. The load on the power stage consists of a 250-W variable power resistor and four 12-V deep-cycle gel cell lead–acid batteries connected in series to achieve a 48-V load bus voltage.

PV array and PV array simulator

Two different power sources were used to test MPPT algorithms. One of these was a 250-W PV array consisting of five series-connected ASE Americas 50-W PV modules. The array's electrical characteristics were: $V_{OC} = 100{\cdot}0$ V, $I_{SC} = 3{\cdot}2$ A, $I_{MPP} = 2{\cdot}8$ A, $V_{MPP} = 86{\cdot}0$ V. These are the manufacturer's rated values under standard operating conditions (irradiance $G = 1000$ W/m^2, AM1·5 solar spectrum, and cell temperature $T = 25°$C). For this work, natural sunlight was used as the irradiance source.

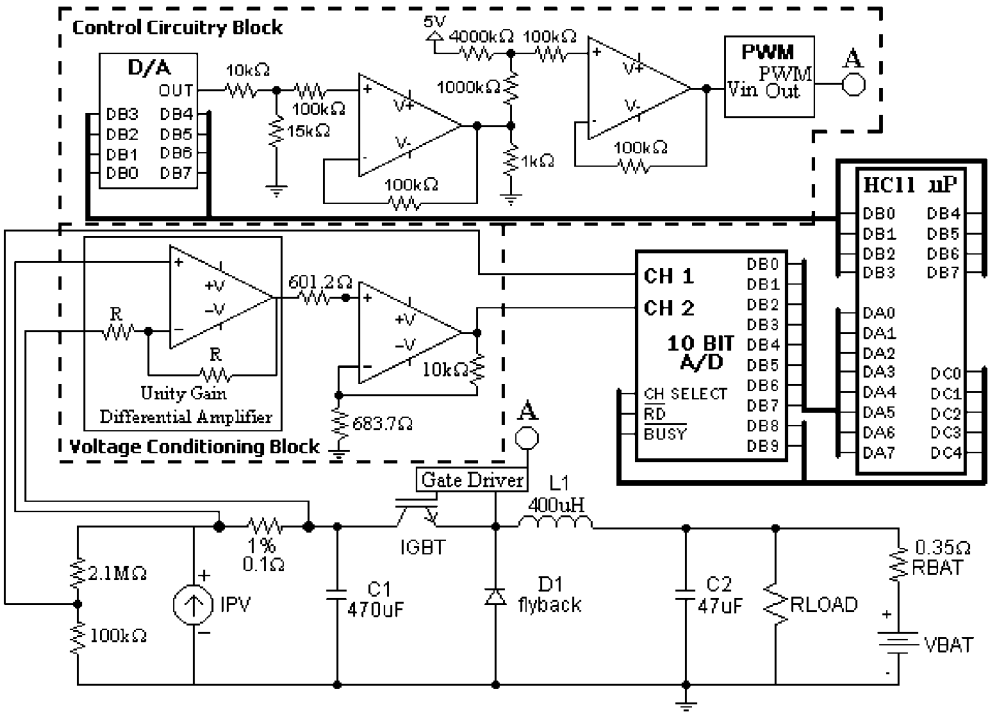

Figure 9. Component level diagram of the MPPT system

To facilitate more controlled tests, experiments were also conducted using an Agilent Technologies solar array simulator (SAS). The simulator's maximum open-circuit voltage and short-circuit current are $V_{OC,\,max} = 120{\cdot}0$ V, $I_{SC,\,max} = 4{\cdot}0$ A, $P_{out,\,max} = 480$ W. The simulator allows simulation of a variety of PV *I–V* curves, within these output constraints. For this work, the simulator was programmed to simulate the *I–V* curve of the actual array described above, with the irradiance profile programmed to mimic a partly cloudy day, the worst case for accurate tracking of the MPP. This irradiance profile is shown as a plot of the simulator's programmed MPP power as a function of time in Figure 10.

Measurement and calculation techniques

The objective of this work is to compare the MPPT efficiencies of the previously described algorithms using Equation (1). Thus, P_{max} and P_{actual} values are needed. For the solar array simulator, this presents no problem; P_{max} is a preprogrammed known value, and P_{actual} can be read off of the simulator.

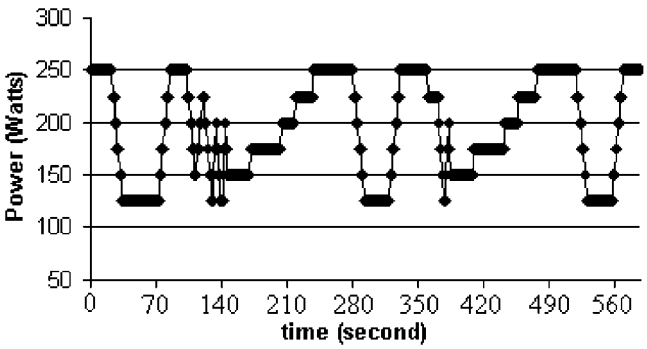

Figure 10. Power curve used to drive the solar array simulator

For the PV array, the situation is more difficult. The PV array P_{actual} was measured directly by a DC power transducer, but finding the value of $P_{\max}$ was problematic. In this study, $P_{\max}$ was calculated using Equation (3) multiplied by voltage. This equation can be differentiated with respect to voltage and set equal to zero, giving $P_{\max}$. However, accurate values of I_{OR}, A, K_1, and R are required. In our array, the series resistance R was very small and was neglected. I_{OR} and A were measured experimentally, using the technique of measuring the array's I–V curve in the dark and plotting it on a semilogarithmic plot. On such a plot, the I–V curve of a PV array typically has two relatively linear regions,[15] arising from the two diodes in the double-exponential model for the solar cell. For PV systems work, it is generally acceptable to use only the region of the curve resulting from the higher voltage $A \simeq 1$ section of the dark I–V curve.[16] A linear fit is made to this region, and the I-axis intercept of this line gives the value of I_{OR} and the value of A can be found from the slope of the line. Two sets of measured data were used, and the results were similar.

The results of the measurements were cross-checked using a three-parameter data fit. Using MATLAB, software was written that examined the measured data and searched for values of I_{OR}, A, and K_1. The allowable ranges of the parameter values were restricted to those that are physically reasonable, and a further constraint was imposed that the MPPT efficiency could never exceed 100%. The MATLAB code swept the three aforementioned parameters over the expected ranges, calculated $P_{\max}$ and the MPPT efficiencies for each set of parameter values and measured data, and found those values that kept the MPPT efficiency below 100%, but as close as possible to the SAS results. There was good correspondence between the measured values and those found using the search.

Based on the measurements and the three-parameter fitting procedure described above, the following values were obtained for the PV array parameters:

$$I_{\text{or}} = 2{\cdot}25\,\mu\text{A}$$
$$K_1 = 0{\cdot}6\,\text{mA}/^{\circ}\text{C}$$
$$A = 1{\cdot}5$$

The plane-of-array irradiance was measured by a Li-Cor silicon photodetector, and the array temperature was measured by a thermocouple attached to the back of the array. All measurements were recorded by a datalogger and used to calculate the quantities P_{actual} and $P_{\max}$. The efficiency of the MPPT algorithm under test was then calculated using Equation (1).

To determine the overall efficiencies of the different algorithms, several trials were run using the PV array and PV simulator. To obtain the overall efficiency of the MPPT algorithm under test using the SAS, five trials were run for each algorithm using the power curve shown in Figure 10. For each trial, the efficiency of the algorithm was calculated using Equation (1). The results were then averaged to obtain the algorithm's overall efficiency. To determine the MPPT efficiencies using the PV array, tests were run on different days with varying illumination intensities and ambient temperatures. To avoid skewing the results, each test consisted of rotating the algorithms at 20-min intervals, operating the system with one algorithm for 20 min, then changing to another algorithm for 20 min, and so on, rotating through all algorithms several times. This was considered the next-best approach to conducting all tests simultaneously, which was not practically possible. The test results for each algorithm were averaged over all testing periods to determine the overall efficiency of the MPPT algorithm.

Several steps were taken to ensure the best performance from the MPPT hardware. For example, all of the MPPT algorithms sampled the array voltage and current at the same instance in the switching period to ensure consistent values of voltage and current. Also, to decrease the amount of noise in the system, each algorithm worked with averages of two sampled voltage and current values.

The sampling rate used in the system also required optimization. To achieve the best performance, the sampling rate was set as fast as possible without causing instability. The instability can arise because of the relatively long time constant (slow dynamics) of the power stage. Depending on the value of the load, the time constant of the power stage varied from 10 to $\sim$50 ms. If the MPPT algorithm were to sample the array voltage and current too quickly, it would in fact be measuring the transient behavior of the power stage, not the desired

steady-state PV array behavior, and the PV array operating point would become unstable as a result. To ensure that the power stage reached the periodic steady state before the next set of voltage and current measurements was taken, a delay was implemented into each algorithm that allowed controllability of the sampling rate. The length of this delay was optimized experimentally by varying it until the MPPT efficiency reached its maximum value under constant PV input.

Finally, it was necessary to optimize the individual parameters of each individual algorithm, so that each achieved its maximum MPPT efficiency. As stated previously, earlier studies, particularly those comparing other algorithms to the P&O method, tend to use a P&O algorithm in which such parameters as increment step size and sampling rate are not discussed, and are possibly not optimized to reflect the true capability of P&O. Thus, in this study each algorithm's parameters were carefully optimized for maximum performance with the hardware described.

Optimal values for the perturbation increment for the P&O and incremental conductance algorithms were found experimentally by observing the overall MPPT efficiencies at different values of these magnitudes for each algorithm, under constant sunlight and also using the simulator. It was found that P&O worked best with a 0·586% step change in the operating point, whereas incremental conductance worked best with a 0·39% change in the operating point. These corresponded to 3-bit and 2-bit changes in the duty cycle respectively. The constant voltage algorithm was optimized by experimentally determining the optimal value of K used in the calculation of V_{OC}. For our PV array under clear sky conditions, we found the optimum K to be 79%.

Unfortunately, testing of the parasitic capacitance MPPT algorithm was not conducted, owing to a difficulty in implementation. As previously stated, the parasitic capacitance algorithm makes use of the fact that the individual solar cells have a *p–n* junction charge storage that can be modeled as a capacitance. The capacitance of the array used in this study was found experimentally by measuring the RC time-constant of the array using a known value of R. An insulated gate bipolar transistor (IGBT) was used to periodically connect the array to a known resistance. When the IGBT was closed, the time it took for the array to reach zero volts was measured. The relationship of $\tau = 1/\mathrm{RC}$ was then used to determine the array's capacitance, which was found to be approximately 66 pF.

However, MPPTs based on buck converters will utilize a large capacitor connected in shunt across the inputs of the MPPT (the output terminals of the PV array). This capacitor is labeled C1 in Figure 9. Note that in the buck converter circuit in Figure 9, the semiconductor switching device (an IGBT, in this case) is in series with the output of the PV array. Thus, when the switch is 'off', acting as an open circuit, the PV array current is interrupted. As the switch is turned on and off, then, the current output of the PV array would have a rectangular pulse waveform if C1 were not present. During the off times of the switch, the PV array would produce no power, and the efficiency of the system would be reduced. To prevent this so-called switching ripple in the MPPT input current from reaching the PV array, the large input capacitor C1 is used to absorb this ripple, leaving (approximately) a pure DC current from the PV array. Unfortunately, the value of this input capacitance is several orders of magnitude larger than the inherent capacitance of the PV array. Thus, the influence of the PV array's capacitance on the power flow of the system was unmeasurable when compared with that of the input capacitor of the MPPT. In order to use the parasitic capacitance method, a different power stage topology (perhaps a boost-based circuit) would be required.

To facilitate comparison between the results of this and other studies,[6] we have separated our results according to the cloudiness conditions under which they were measured. A test run was classified as a 'clear sky' run if fewer than six 100-W power transients and an average irradiance of over 600 W/m^2 were observed. If there were fewer than six 100-W power transients and the average irradiance was less than 600 W/m^2, the run was classified as 'cloudy'. If there were more than six 100-W transients in power, the conditions were classified as 'partly cloudy'.

RESULTS

A typical example of the data collected in this study is shown in Figure 11, in which the theoretical power P_{TH} and the actual power P_{ACT} are both plotted. This test run was conducted on a clear day, the power source was the PV array, and the MPPT was under the control of the P&O algorithm. As might be expected under these

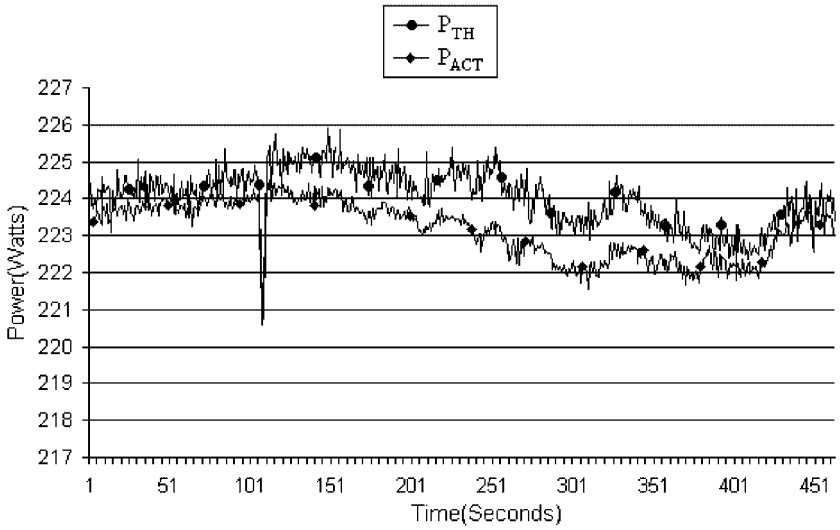

Figure 11. Typical example of the data collected in this study

conditions, the actual power P_{ACT} tracks the theoretical power P_{TH} very closely, with a maximum deviation of about 1 W. The small downward spike in the test run shown in Figure 11 was caused by human interference with the array (accidental shadowing by a passerby).

A summary of the MPPT efficiencies (η_{MPPT}) of the different algorithms is shown in Table II. The three algorithms for which results are given are perturb and observe (P&O), constant voltage (CV), and incremental conductance (INC). All efficiencies are based on at least six days' worth of data, as shown in Table II. The highest efficiencies are generally obtained with the incremental conductance algorithm. Also, the efficiencies obtained using the PV simulator are a few tenths of a percent higher than those obtained using the PV array, but are very close in all cases.

The level of error in the SAS results is expected to be less than 1%, and arises from the measurement error in the SAS output voltage and current and the SAS theoretical power. The level of error in the results from the PV array will be somewhat higher, due to the higher number of different measurements, but is believed to be $\leqslant 4\%$. Also, there will be some error in the absolute value of the MPPT efficiencies found using the PV array due to error in I_{or}, K_1, and A. However, as the values used for these parameters are entirely reasonable in terms of past experience and manufacturer's expectations, this error should be small and confidence in these values is warranted. Also, it should be borne in mind that the objective of this work was to obtain the relative comparison between the methods, and this relative comparison should be unaffected by any error in I_{or}, K_1, and A.

The erratic behavior of the P&O algorithm under rapidly changing irradiance conditions predicted by earlier studies[6] was observed in this study as well. An example of this behavior is shown in Figure 12. This figure

Table II. Overall MPP tracking efficiencies (η_{MPPT})

Sky conditions	P&O		Inc		CV	
PV array	Days of data	η_{MPPT}	Days of data	η_{MPPT}	Days of data	η_{MPPT}
Clear	20	98·7	17	98·7	20	90·4
Partly cloudy	14	96·5	11	97·0	10	90·1
Cloudy	9	98·1	11	96·7	6	93·1
Overall	43	97·8	39	97·4	36	91·2
Simulator						
Overall	99·3		99·4		93·1	

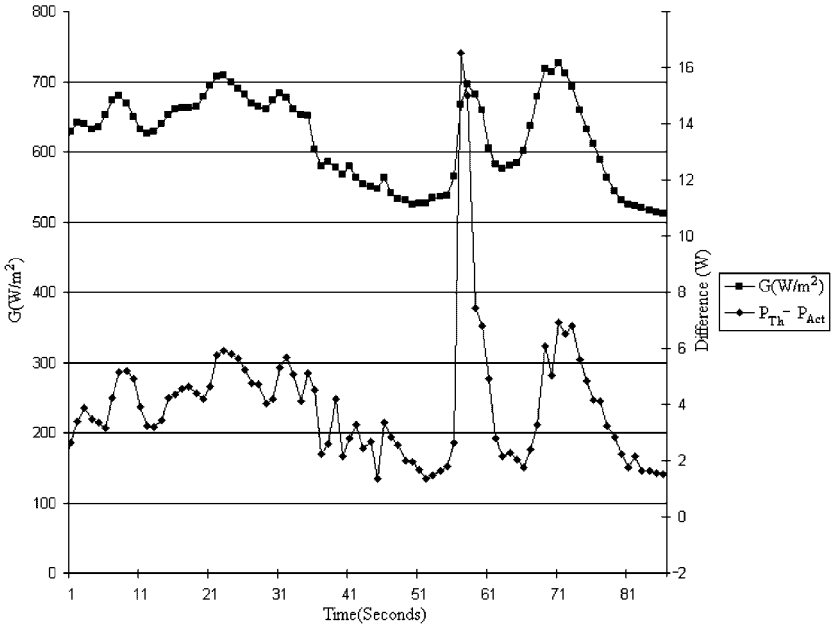

Figure 12. Data demonstrating the erratic behavior of the P&O algorithm under rapidly changing irradiance

shows the irradiance G and the error between the theoretical maximum power and the actual power ($P_{TH} - P_{ACT}$) as functions of time, during a P&O-controlled run. There is a significant transient in the irradiance about 57 s into the run. At that point, there is a large upward spike in the power error as the P&O algorithm initially tracks in the wrong direction (see Figure 4). A few seconds later there is a second transient, and a similar (but smaller) surge in the power error.

DISCUSSION

We believed at the outset of this study that we would find that the perturb-and-observe and incremental conductance algorithms should have very similar overall efficiencies, but that incremental conductance should be slightly better. However, the results of this study indicate that, to within the accuracy available, the MPPT efficiencies of the incremental conductance and perturb-and-observe MPPT algorithms are essentially the same. When optimized for the particular MPPT hardware in use, P&O and INC had the same performance under clear sky conditions, indicating that the penalty in efficiency caused by the oscillation about the MPP inherent in P&O under steady-state conditions was insignificant for the optimized algorithms. Incremental conductance outperformed P&O under partly cloudy conditions, as expected, but the difference was very small. Also, interestingly, P&O had a significantly higher efficiency than incremental conductance under cloudy skies. The reason for this can be understood through the array P–V curves in Figure 3 and one of the relations used by the incremental conductance algorithm, given in Equation (7a). Because of such factors as measurement error and noise, if the microcontroller required the two sides of Equation (7a) to be exactly equal, then that equation would never be satisfied. Thus, in practice Equation (7a) is considered satisfied if its two sides are within a small range of each other. However, as seen in Figure 3, when the array voltage is changed the resulting change in power is very small. Thus, at low irradiances, in the range of voltages near V_{MPP}, Equation (7a) is usually approximately satisfied, and the incremental conductance algorithm gets 'stuck' at an operating voltage that is not quite the same as V_{MPP}.

It is also interesting to note that the efficiencies of both the P&O and incremental conductance algorithms can be quite high, well in excess of 97% when properly optimized. The results suggest that the simplicity of the

P&O algorithm may outweigh any advantage offered by incremental conductance in most applications, particularly low-cost applications such as module-integrated power electronics. The P&O method can be implemented with fairly simple analog circuitry or a very-low-cost microcontroller. Incremental conductance, on the other hand, requires differentiation, division circuitry and a relatively complex decision making process, and therefore requires a more complex microcontroller with more memory. The choice of which of these two MPP tracking algorithms to use in a PV system can be made by weighing the increased cost of the MPPT to the overall increase of energy produced. This would suggest that an increase in MPPT cost might be justified in a larger PV system, where a small percentage increase in efficiency would lead to a significant increase in energy output. This is the subject of ongoing work.

It should also be mentioned that MPPT algorithms based on digital signal processing (DSP) or fuzzy logic have recently received widespread attention. Preliminary results indicate that MPPT efficiencies for these algorithms can be very high.[17,18] These were not included in this study, owing to their cost of implementation. However, in the future, as their implementation costs decrease, these methods could become feasible. It is possible that such algorithms might be attractive even now in very large, high-power PV systems, because in those cases a few tenths of a percent improvement in MPPT efficiency could translate into a large improvement in energy output that might offset the higher cost of the MPPT. (The relevance of this advantage is debatable, as many believe PV systems of such size are not a likely mode of PV deployment.) Further investigation of the MPPT efficiencies of these algorithms is warranted.

CONCLUSIONS

This study presents an experimental comparison of the maximum power point tracking efficiencies of several MPPT control algorithms that are discussed in the literature. The scope of the study was limited to those algorithms thought to be applicable to low-cost implementations with currently available hardware. The results suggest that, on the basis of maximum power point tracking efficiency, the perturb-and-observe method, already by far the most commonly used algorithm in commercial converters, has the potential to be very competitive with other methods *if* it is properly optimized for the given hardware. Incremental conductance performed as well as P&O, but in general its higher implementation cost would not be justified by any improvement in performance. The parasitic capacitance method could not be implemented in our experimental set-up, and some doubt exists as to whether it could be implemented in most commercial PV power converters because of the use of large input capacitors. Finally, as expected, the MPPT efficiency increases gained by using the perturb-and-observe and incremental conductance algorithms make them favorable over the simpler constant voltage method.

REFERENCES

1. Katan RE, Agelidis VG, Nayar CV. Performance analysis of a solar water pumping system. *Proceedings of the 1996 IEEE International Conference on Power Electronics, Drives, and Energy Systems for Industrial Growth (PEDES)*, 1996; 81–87.
2. Taha MS, Suresh K. Maximum power point tracking inverter for photovoltaic source pumping applications. *Proceedings of the 1996 IEEE International Conference on Power Electronics, Drives, and Energy Systems for Industrial Growth (PEDES)*, 1996; 883–886.
3. Kourtoulis E, Kalaitzakis K, Voulgaris NC. Development of a microcontroller-based, photovoltaic maximum power point tracking control system. *IEEE Transactions on Power Electronics* 2001; **16**(1): 46–54.
4. Won C-Y, Kim D-H, Kim S-C, Kim W-S, Kim H-S. A new maximum power point tracker of photovoltaic arrays using fuzzy controller. *Proceedings of the 24th IEEE Power Electronics Specialists Conference (PESC)*, 1994; 396–403.
5. Hua C, Shen C. Comparative study of peak power tracking techniques for solar storage systems. *IEEE Applied Power Electronics Conference and Exposition—APEC, Proceedings of the 1998 13th Annual Applied Power Electronics Conference and Exposition* 1998; **2**: 697–685.
6. Hussein KH, Zhao G. Maximum photovoltaic power tracking: an algorithm for rapidly changing atmospheric conditions. *IEE Proceedings of Generation, Transmission, Distribution* 1995; **142**(1): 59–64.

7. Kim Y, Jo H, Kim D. A new peak power tracker for cost-effective photovoltaic power systems. *IEEE Proceedings* 1996; **3**(1): 1673–1678.
8. Kawamura T, *et al.* Analysis of MPPT characteristics in photovoltaic power systems. *Solar Energy Materials and Solar Cells, Proceedings of the 1996 9th International Photovoltaic Science and Engineering Conference*, *PVSEC-9* 1997; **47**(14): 155–165.
9. Enslin JHR, Wolf M, Swiegers W. Integrated photovoltaic maximum power point tracking converter. *IEEE Transactions on Industrial Electronics* 1997; **44**(6): 769–773.
10. Andersen M, Alvsten B. 200W low cost module integrated utility interface for modular photovoltaic energy systems. *IECON: Proceedings of the 1995 IEEE 21st International Conference on Industrial Electronics, Control and Instrumentation* 1995; **1**(1): 572–577.
11. van der Merwe L, van der Merwe G. Maximum power point tracking—implementation strategies. *Proceedings of the IEEE International Symposium on Industrial Electronics* 1998; **1**(1): 214–217.
12. Abou El Ela M, Roger J. Optimization of the function of a photovoltaic array using a feedback control system. *Solar Cells: Their Science, Technology, Applications and Economics* 1984; **13**(2): 185–195.
13. Salameh Z, Dagher F, Lynch W. Step-down maximum power point tracker for photovoltaic systems. *Solar Energy* 1991; **46**(5): 279–282.
14. Brambilla A, *et al.* New approach to photovoltaic arrays maximum power point tracking. *Proceedings of the 30th IEEE Power Electronics Conference*, 1998; 632–637.
15. Hovel HJ. *Semiconductors and Semimetals: Solar Cells.* Academic Press: New York, 1975; 64ff.
16. Fraas LM, Avery JE, Gruenbaum PE, Sundaram VS. Fundamental characterization studies of GaSb solar cells. *Proceedings of the IEEE Photovoltaic Specialists Conference*, 1991; 80–84.
17. Hua C, Lin J, Shen C. Implementation of a DSP-controlled photovoltaic system with peak power tracking. *IEEE Transaction on Industrial Electronics* 1998; **45**(1): 99–107.
18. Won C-Y, Kim D-H, Kim S-C, Kim W-S, Kim H-S. New maximum power point tracker of photovoltaic arrays using fuzzy controller. *Proceedings of the 1994 25th Annual IEEE Power Electronics Specialists Conference* 1994; **2**: 396–403.

